Replication initiation in bacteria: precision control based on protein counting

Haochen Fu† and Fangzhou Xiao†
Department of Physics, University of California San Diego, 9500 Gilman Dr, La Jolla, CA 92093

Suckjoon Jun*
Department of Physics and Department of Molecular Biology, University of California San Diego, 9500 Gilman Dr, La Jolla, CA 92093

Balanced biosynthesis is the hallmark of bacterial cell physiology, where the concentrations of stable proteins remain steady. However, this poses a conceptual challenge to modeling the cell-cycle and cell-size controls in bacteria, as prevailing concentration-based eukaryote models are not directly applicable. In this study, we revisit and significantly extend the initiator-titration model, proposed thirty years ago, and explain how bacteria precisely and robustly control replication initiation based on the mechanism of protein copy-number sensing. Using a mean-field approach, we first derive an analytical expression of the cell size at initiation based on three biological mechanistic control parameters for an extended initiator-titration model. We also study the stability of our model analytically and show that initiation can become unstable in multifork replication conditions. Using simulations, we further show that the presence of the conversion between active and inactive initiator protein forms significantly represses initiation instability. Importantly, the two-step Poisson process set by the initiator-titration step results in significantly improved initiation synchrony with $CV \sim 1/N$ scaling rather than the standard $1/\sqrt{N}$ scaling in the Poisson process, where N is the total number of initiators required for initiation. Our results answer two long-standing questions in replication initiation: (1) Why do bacteria produce almost two orders of magnitude more DnaA, the master initiator proteins, than required for initiation? (2) Why does DnaA exist in active (DnaA-ATP) and inactive (DnaA-ADP) forms if only the active form is competent for initiation? The mechanism presented in this work provides a satisfying general solution to how the cell can achieve precision control without sensing protein concentrations, with broad implications from evolution to the design of synthetic cells.

I. INTRODUCTION

Most biology textbooks explain biological decision-making by emphasizing the control and sensing of key protein concentrations through programmed gene expression and protein degradation in eukaryotes. Protein concentration gradients can encode spatial or temporal information across different scales, such as morphogen gradients in the French flag model in developmental biology [1] or cyclin oscillations in eukaryotic cell-cycle controls [2] [Fig. 1(a)]. However, in bacterial cell physiology, balanced biosynthesis has been the hallmark since the 1950s at the population and single-cell levels. Balanced biosynthesis means that the synthesis rate of all cellular components is the same as the cell's growth rate in steady-state growth, wherein the concentrations of stable proteins are steady by the balance of their production and dilution [3–5] [Fig. 1(b)].

However, balanced biosynthesis poses a fundamental conceptual challenge to modeling the cell-cycle and cell-size controls, as the prevailing concentration-based models are not directly applicable if the concentration of cell-cycle proteins remains constant (within stochasticity). Indeed, for the billion-year divergent model bacterial organisms *Escherichia coli* and *Bacillus subtilis*, their size control is based on (1) balanced biosynthesis of division initiator protein FtsZ and (2) its accumulation to a threshold number (not concentration) [6]. These two conditions lead to the adder phenotype [6]. Unfortunately, a mechanistic investigation of threshold FtsZ number sensing is a formidable challenge because division initiation involves multiple interacting proteins with unknown properties [7].

Replication initiation in bacteria, which is exclusively controlled by the widely-conserved master regulator protein, DnaA, is an attractive problem for mechanistic investigation because it exhibits the adder phenotype [8–11] and must require accumulation to a threshold number of DnaA [6]. Furthermore, DnaA has been extensively studied, and most properties required for modeling are known or can be estimated [12–14]. Therefore, we view *E. coli* replication initiation as a tractable problem to understand the mechanism of protein copy-number sensing to control the cell cycle, and gain insight into the general class of precision control in biology.

In this work, we revisit and significantly extend the initiator-titration model proposed by Hansen, Christensen, and Atlung thirty years ago [15], the model closest to the protein-number-sensing idea (see Section A). In Section A, we summarize the original initiator-titration model and introduce our initiator-titration model v2. In Section B, we first introduce the "protocell" model, a minimal version of the initiator-titration model, and derive the first expression of the protocell size at initiation

* Corresponding author: suckjoon.jun@gmail.com
†These authors contributed equally to this work.

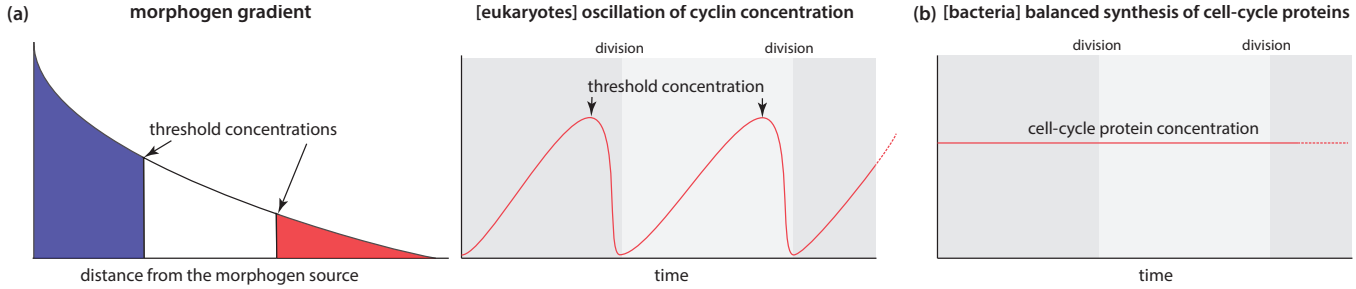

FIG. 1. Protein concentration in eukaryotes vs. bacteria. (a) (left) morphogen gradient in the French flag model in developmental biology. (right) Oscillation of cyclin concentration for eukaryotic cell-cycle control. (b) Balanced biosynthesis in bacteria.

(known as the "initiation mass"). In Section C, we perform a dynamical stability analysis of the protocell model and show the existence of initiation instability. In Section D, we extend the protocell to our "initiation-titration model v2" and derive an analytical expression for the initiation mass in a special case (the $\Delta 4$ mutant [16]) based on three mechanistic biological control parameters: the expression level of DnaA, the ratio of the active vs. passive forms of DnaA, namely, [DnaA-ATP]/[DnaA-ADP], and the number of DnaA titration boxes on the chromosome. In the same section, we show that adding the replication-dependent, biologically-observed DnaA-ATP $\rightarrow$ DnaA-ADP conversion element (RIDA) restores stability in the model by simulation [17, 18]. In Sections E and F, we explain asynchrony (intrinsic noise) and cell-to-cell variability (extrinsic noise) using the initiation-titration model v2.

Our model provides a quantitative and mechanistic explanation for several long-standing questions in bacterial replication initiation with the following findings: DnaA titration boxes are the protein-counting device that measures the threshold number of initiator proteins, and the two forms of DnaA (DnaA-ATP and DnaA-ADP), and especially the replication-dependent DnaA-ATP $\rightarrow$ DnaA-ADP, are needed to suppress initiation instability. Given the fundamental nature of replication initiation and its profound differences from eukaryotic cell-cycle control, we anticipate broad applications of our results, from the design of synthetic cells to the evolution of biological mechanisms in precision control.

II. RESULTS AND DISCUSSION

A. The "initiator-titration model v2" and intuition

Consider engineering a synthetic cell capable of self-replication. For such a cell to be viable, it must meet a fundamental requirement of cell-cycle control: initiating replication only once during cell division. A possible "simple" strategy to implement this requirement could be as follows [Fig. 2(a)]: (1) The chromosome has one origin of replication. (2) The cell produces one initiator protein during the division cycle. (3) The initiator protein binds to the ori and immediately triggers initiation. (4) Upon initiation, the cell destroys the initiator protein. While this seemingly straightforward strategy could limit the replication origin to a single site and produce a single initiator protein during cell division, the underlying mechanisms required to achieve this are likely more complex. For instance, how would the cell "count" the number of initiator proteins and "know" when to degrade them?

While *E. coli* exhibits characteristics similar to the hypothetical strategy described above, there are notable differences. *E. coli* has one replication origin (*ori*), but replication initiation requires 10-20 master regulator DnaA molecules binding to the eleven DnaA boxes at *ori*. Furthermore, DnaA is stable and not degraded upon initiation [13, 14, 19, 20]. Strikingly, *E. coli* produces approximately 300 copies of DnaA per *ori*, or 30 times more than required at *ori*, with almost all being titrated by DnaA boxes encoded in the chromosome [13, 14, 19, 20].

In 1991, Hansen and colleagues proposed the initiator-titration model to explain these observations [Fig. 2(b)] [15]. Their model posits that DnaA is first titrated by high-affinity DnaA boxes in the chromosome, which allows it to bind to *ori* with weak affinity and initiate replication only after the chromosomal DnaA boxes are nearly saturated. This highlights the importance of DnaA boxes in the chromosome as the timing device for replication initiation.

Our model builds upon the initiator-titration model and incorporates the knowledge in DnaA accumulated in the past 30 years [13, 14, 19, 20]. Specifically, we have learned that DnaA exists in two forms, DnaA-ATP and DnaA-ADP, with different binding affinities to DNA. DnaA-ATP is the active form that can trigger initiation, while DnaA-ADP is inactive. Further genetic, biochemical, and bioinformatic studies have revealed that approximately 300 high-affinity DnaA boxes are distributed across the circular chromosome. By contrast, only three of the eleven DnaA boxes in the *ori* region are high-affinity sites. Therefore, most DnaA, whether DnaA-ATP or DnaA-ADP, will first bind the high-affinity chromosomal DnaA boxes before initiating replication at *ori*. We refer to this updated model as the Initiator-titration model v2, in recognition of the pioneering work of Hansen

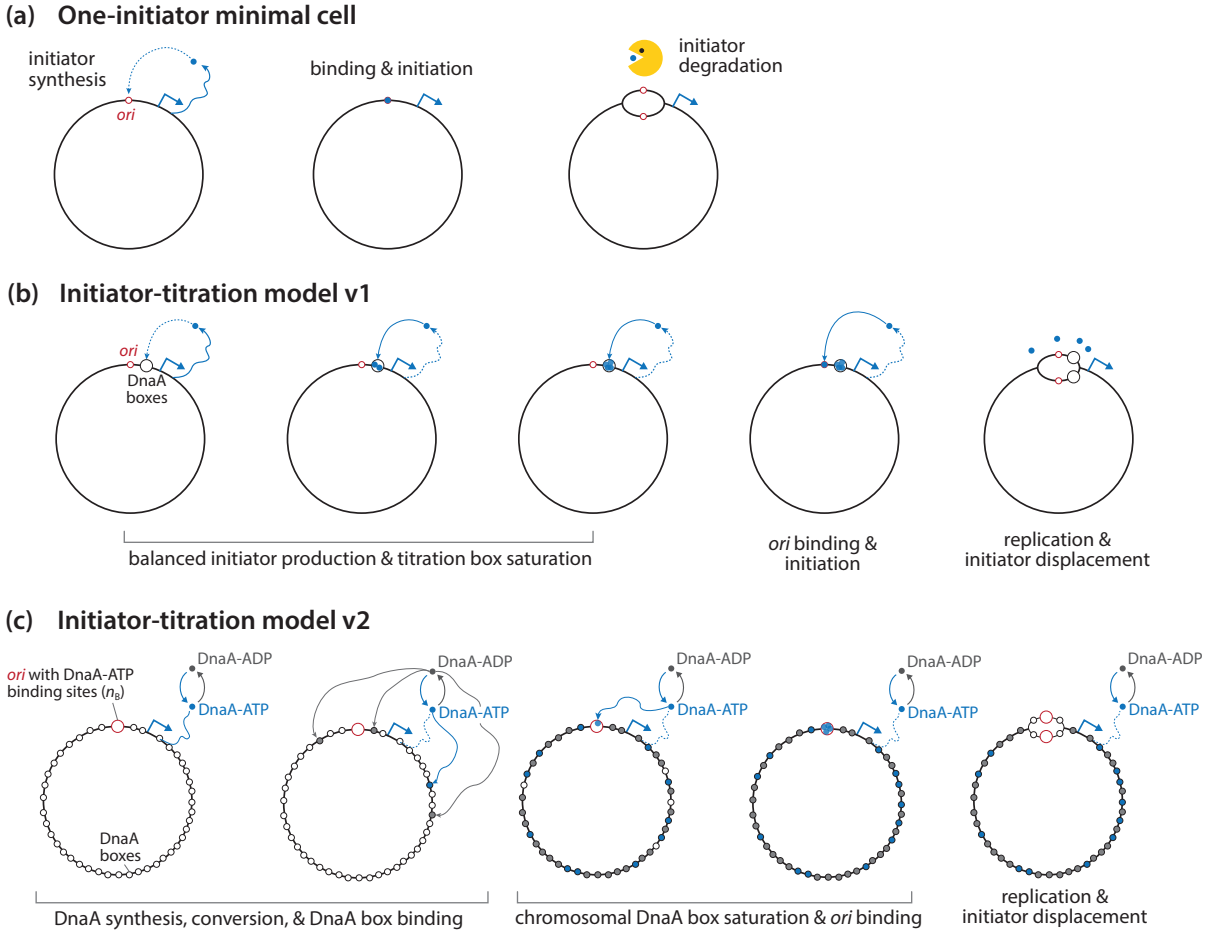

FIG. 2. Initiation control. (a) Hypothetical minimal cell. (b) Initiator-titration model v1 [15]. (c) Initiator-titration model v2 (this work).

et al.

Figure 2(c) illustrates how our initiator-titration model v2 works in more detail. To provide intuition without losing the generality of our ideas, let us consider a naked circular chromosome without bound DnaA.

1. As the cellular concentration of ATP is almost 10x higher than ATP, newly synthesized DnaA becomes DnaA-ATP. The conversion between DnaA-ATP and DnaA-ADP is slow (namely, comparable to the timescale of cell-doubling time) such that the DnaA-ATP:DnaA-ADP ratio is maintained stably, approximately 1:3 in wildtype *E. coli* [14].

2. Both DnaA-ATP and DnaA-ADP will bind the chromosomal DnaA boxes first since the chromosome contains 100x more high-affinity DnaA boxes than *ori* (300 vs. 10).

3. When most chromosomal DnaA boxes are saturated, the probabilities for DnaA-ATP binding to *ori* vs. the remaining chromosomal DnaA boxes become comparable. Since DnaA-ADP is present 3x more than DnaA-ATP and can bind the chromosomal DnaA boxes, *ori* becomes quickly saturated by DnaA-ATP, and replication initiates.

As we elaborate below, the initiator-titration model v2 answers two long-standing fundamental questions:

1. Why does *E. coli* maintain two forms of DnaA in the first place if they only need DnaA-ATP for initiation?

2. Why does *E. coli* produce so much more DnaA proteins than required for initiation, only to be titrated?

B. The "protocell": minimal initiator-titration model

To gain analytical insight, we first construct a minimal initiator-titration model [Fig. 3(a)]. This "protocell" has the complexity between the two versions of the initiator-titration model [Figs. 2(b) & 2(c)]. The protocell has the replication origin (*ori*), the initiator protein

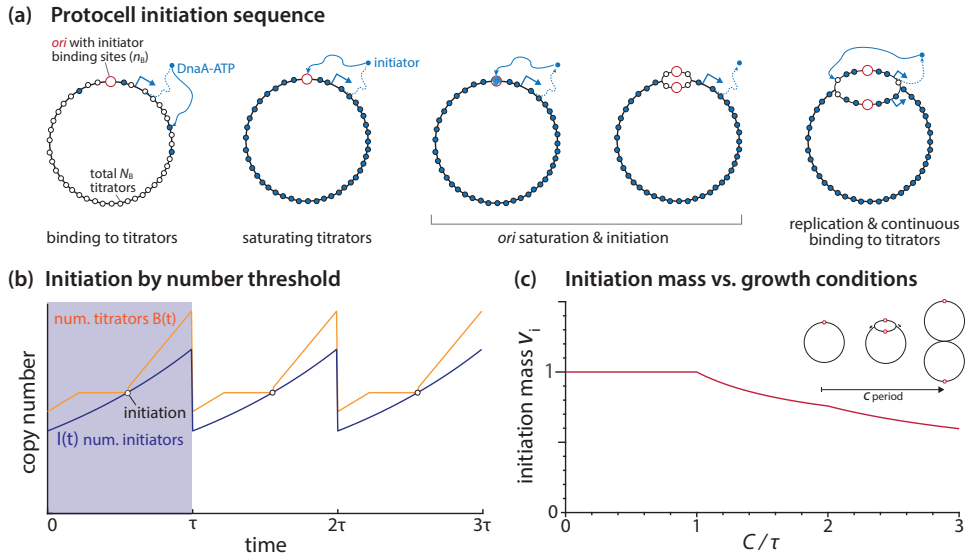

FIG. 3. Initiation control of protocell by initiator number threshold. (a) Model sequence of titration and initiation. (b) Change in the initiator and titrator copy numbers during the cell cycle, and the initiation condition $I(t) = B(t)$. (c) Predicted initiation mass in different growth conditions (C/τ). $n_B/N_B = 1/30$.

(e.g., DnaA in *E. coli*), and the initiator binding site on the chromosome (DNA sequence with a strong affinity for the initiator such as the 300 DnaA boxes in the *E. coli* chromosome). We assume the following based on experimental data:

1. The cell grows exponentially $V(t) = V_0 e^{\lambda t}$ in steady-state, where $V(t)$ is the total cell size at time t, and λ is the growth rate. The mass-doubling time τ is given by $\tau = \frac{\ln 2}{\lambda}$.

2. Synthesis of the initiator protein is balanced, i.e., its concentration is constant during growth [3]. We denote the initiator protein copy number at time t as $I(t)$ and its concentration as c_I.

3. The rate of DNA synthesis is constant [6], with the duration of chromosome replication C.

4. The chromosome encodes specific DNA sequences for binding of the initiator proteins. n_B low-affinity sites are localized at *ori* and N_B high-affinity sites are evenly distributed on the chromosome. For the *E. coli* chromosome, $N_B \approx 300$ and $n_B \approx 10$. During replication, the number of initiator binding sites increases as $B(t)$.

5. Initiators tightly bind to the binding sites rather than staying in the cytoplasm, and initiators preferentially bind to the chromosomal binding sites before binding to the ones at *ori*. Therefore, replication initiates at $t = t_{ini}$ when $I(t) = B(t)$, namely, all binding sites are saturated by the initiator proteins.

For illustration purposes, we consider an intermediate growth condition, where two cell cycles slightly overlap without exhibiting multifork replication [21] (Fig. 3). In the Helmstetter-Cooper model [22], this corresponds to $C < \tau < C + D$, where D is the duration between replication termination and cell division.

The steady-state curves of $I(t)$ and $B(t)$ are shown in Fig. 3(b) (In our model, a steady state means all derived quantities are periodic with a period of τ). In general, $I(t)$ increases exponentially because of exponential growth and balanced biosynthesis (Assumptions 1&2 above), whereas $B(t)$ increases piecewise linearly because of replication initiation and termination (see also Assumptions 3&4). Therefore, the number of initiators will catch up with the total number of binding sites between replication termination and the new round of initiation when $I(t = t_{ini}) = B(t = t_{ini}) = 2(N_B + n_B)$, and initiation is triggered based on Assumption 5. Upon initiation, the number of binding sites $B(t)$ increases discontinuously by $2n_B$ due to the duplication of *ori* and the binding sites therein. After that, $B(t)$ increases at the rate $2N_B/C$, steeper than the slope of $I(t)$. After cell division, $I(t)$ and $B(t)$ drop by half, and the cell repeats its cycle.

From this picture, the initiation mass, defined by cell volume per *ori* at initiation, can be easily calculated by the number of initiators at initiation,

$$v_i = \frac{I(t_{ini})}{2c_I} = \frac{1}{c_I}(N_B + n_B),$$

where "2" reflects the copy number of *ori* before initiation.

The above result can be extended to different growth conditions. For example, in slow growth ($\tau > C + D$), the initiation mass is the same as in the intermediate condition, because replication cycles do not overlap in both conditions. In fast-growth conditions ($\tau < C$), replication cycles overlap, exhibiting multifork replication. Since a new round of replication starts before the previous round of replication is completed, the initiation mass is given by

$$v_i = \frac{1}{c_I}(\alpha N_B + n_B), \quad (1)$$

with the cell-cycle dependent parameter $\alpha \leq 1$ given as

$$\alpha = \frac{1}{2^n} + \left(2 - \frac{n+2}{2^n}\right)\frac{\tau}{C}, \quad n = \lfloor \frac{C}{\tau} \rfloor. \qquad (2)$$

See Appendix A for a derivation. Some of the most salient predictions of these results include (1) The initiation mass is inversely proportional to the initiator concentration c_{I} (2) The initiation mass linearly depends on the number of chromosomal binding sites N_{B}.

The basis of the protocell's behavior is that the initiator increases exponentially, whereas the number of binding sites increases piecewise linearly only during DNA replication. Therefore, the cell always reaches the initiation point $I(t) = B(t)$, followed by the titration period, as explained above.

C. The protocell exhibits initiation instabilities.

In the last section, we addressed if a solution exists in the minimal protocell model with a period of τ. We showed that this periodic solution always exists. We defined it as the "steady-state" solution in the biological sense that the cell can grow in a steady state with the periodic cell cycle. However, the model is dynamic, and convergence to a steady state from a given initial condition, $I(0)$ and $B(0)$, is not guaranteed. Hence, in this section, we study how the replication cycle propagates in the lineage from an arbitrary initiation condition at $t = 0$, and under what conditions the cycle converges to the steady-state solution.

Intuitively, if the two consecutive initiations are separated by τ, thus periodic, the system is in a steady state. Suppose an initiation event is at $t = 0$, and its initiation mass deviates from the steady-state solution Eq. 1. Typically, the next initiation occurs at $t = t^+ \neq \tau$. However, if this time interval between two consecutive initiations eventually converges to τ, the steady-state solution is stable under perturbations on the initial conditions. Otherwise, the steady-state solution is unstable. Understanding the stability condition is critical from a biological perspective, because unstable initial control can lead to re-initiations or loss of chromosomes, namely, cell death.

In the rest of this section, we study a dynamical system mathematically based on Assumptions 1-5 in Section B on protocell.

1. *Setup*

We consider a protocell containing one chromosome with ongoing multifork replication [Fig. 3(a)]. We block the cell division so the protocell grows indefinitely as the chromosome replicates and multiplies starting from the initial condition. As the cell size reaches infinity, does the initiation mass have a fixed value (stable) or multiple values (unstable)? The analysis is non-trivial, as we need to accommodate arbitrary initial conditions.

To this end, we start with ordinary differential equations. First, we have

$$\frac{\mathrm{d}I}{\mathrm{d}t} = \lambda I,$$

which describes cell growth and balanced biosynthesis of the initiator proteins. Next, the dynamics of $B(t)$ is more subtle because it increases piecewise linearly depending on the replication state of the chromosome and the number of replication forks. To accommodate the possibility of arbitrary initial conditions, we will define the "multifork tracker" vector variable, $\boldsymbol{\rho}(t)$, as follows.

$$\boldsymbol{\rho}(t) \equiv \begin{cases} [\rho_1(t), \rho_2(t), \cdots, \rho_{\mathrm{d}}(t)], & \text{if} \quad d \geq 1, \\ 0, & \text{if} \quad d = 0. \end{cases} \qquad (3)$$

Here, the index d is the total number of generations (namely, the total rounds of replication cycles) since the initial chromosome, so d can grow indefinitely. That is, at every new round of the replication cycle, the size of the vector increases by one from d to $d + 1$. $d = 0$ is for the initial cell if it had an intact single chromosome without ongoing replications.

We use the variable ρ to indicate the relative position of a pair of replication forks between *ori* and *ter*, and therefore $0 \leq \rho(t) \leq 1$ [Fig. 3(b)]. For example, ρ would be 0.5 if the pair of foks is exactly halfway between *ori* and *ter* [Figs. 3(a) and 3(b)]. To track multifork replication, we need $\rho_{\mathrm{i}}(t)$, where $0 \leq i \leq \lfloor \frac{C}{\tau} \rfloor$, for the i-th pair of replication forks closest to the *ori* [Fig. 3(a)]. Therefore, when $d > \lfloor \frac{C}{\tau} \rfloor$, $\rho_{\mathrm{i}}(t) = 1$ since the replication forks had already reached *ter*.

Based on the "multifork tracker" vector, the number of binding sites $B(t)$ is completely determined by $\boldsymbol{\rho}$ as

$$B[\boldsymbol{\rho}(t)] = N_{\mathrm{B}}\left[1 + \sum_{i=1}^{d} \rho_{\mathrm{i}}(t) 2^{d-i}\right] + 2^d n_{\mathrm{B}}. \qquad (4)$$

The dynamics of $\boldsymbol{\rho}(t)$ consists of two parts: First, between two initiation events, $\rho_{\mathrm{i}}(t)$ increases linearly with a slope of $1/C$ until they reach 1 [Fig. 3(b)]. Second, at initiation, the dimension of $\boldsymbol{\rho}$ increases by one, shifting its components to the right as $S : \mathbb{R}^d \to \mathbb{R}^{d+1}$, $(\rho_1, \rho_2, \cdots, \rho_d) \mapsto (0, \rho_1, \rho_2, \cdots, \rho_d)$ to accommodate the new pair of replication forks at *ori* [see, also, Fig. 3(a)].

2. *Properties of the steady state*

The steady-state solution assumes periodicity of dynamics so that $I(t)$ and $B(t)$ double in each replication cycle. We consider the mapping between two consecutive initiation events to solve for the steady-state condition. We denote the first initiation event as $\boldsymbol{\rho}(t = 0) = \boldsymbol{\rho}$ at $t = 0$, and the second initiation event as $\boldsymbol{\rho}(t = t^+) = \boldsymbol{\rho}^+$

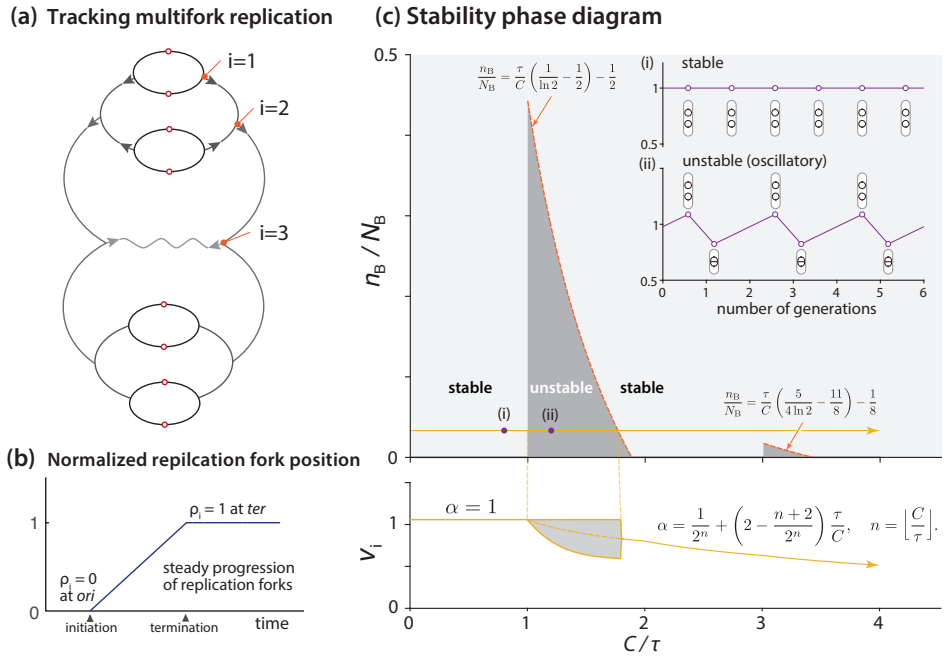

FIG. 4. Dynamical stability analysis for initiation of the protocell. (a) Multifork replication tracker. $i = 1$ is the pair of replication forks closest to *ori*. (b) Linear (in time) progression of the replication forks from *ori* to *ter* of on the circular chromosome. *ter* is on the opposite end of *ori* on the chromosome. (c) Stability phase diagram (n_B/N_B vs. C/τ space). Inset: stable initiation events vs. unstable (oscillatory) initiation events.

at $t = t^+$. The mapping $\mathcal{F} : \mathbb{R}^{d-1} \to \mathbb{R}^d, \boldsymbol{\rho} \mapsto \boldsymbol{\rho}^+$ requires a time-translation and a shift:

$$\rho_i^+ = \begin{cases} \rho_{i-1} + \frac{t^+}{C}, & \text{if} \quad \rho_{i-1} + \frac{t^+}{C} < 1, \\ 1, & \text{else}, \end{cases} \tag{5}$$

where the initiation time t^+ is determined by the requirement $I(t) = B(t)$,

$$\frac{e^{\lambda t^+}}{2}\left\{N_B\left[2^{-(d-1)} + \sum_{i=1}^{d-1}\rho_i 2^{-i}\right] + n_B\right\} = N_B\left(2^{-d} + \sum_{i=1}^{d}\rho_i^+ 2^{-i}\right) + n_B. \tag{6}$$

Eqs. 5 & 6 describe the dynamics of the system at initiation. We can now obtain the fixed point of the mapping $\mathcal{F}$ by setting $d \to \infty$ and $\boldsymbol{\rho}^+ = \boldsymbol{\rho}$:

$$t^+ = \tau, \quad \rho_i^{\text{ss}} = \begin{cases} i\frac{\tau}{C}, & \text{if} \quad i \le \lfloor \frac{C}{\tau} \rfloor, \\ 1, & \text{else}. \end{cases} \tag{7}$$

The resulting expression for steady-state initiation mass is the same as Eq. 1, i.e., the fixed point of $\mathcal{F}$ is the steady-state solution (see Appendix B for more details).

Next, we study the stability of the fixed point of $\mathcal{F}$ by calculating the Jacobian matrix of $\mathcal{F}$ at the fixed point:

$$J = \left.\frac{\partial \rho_i^+}{\partial \rho_j}\right|_{\text{ss}}. \tag{8}$$

This matrix can be reduced to an $n \times n$ matrix ($n = \lfloor \frac{C}{\tau} \rfloor$), since all other matrix elements are zero. In *E. coli*, $0 \le n \le 3$ in most growth conditions, e.g., fastest-growing cells double mass at every $\tau = 10$ minutes, and the C period is 40 minutes. Therefore, we can calculate the eigenvalues of J for each n. Stability requires the highest eigenvalue of J to be smaller than 1. Eventually, we can obtain the stable and unstable regimes in the n_B/N_B vs. C/τ phase diagram, as shown in Fig. 3(c) (see Appendix B, also Fig. S2). Importantly, the phase diagram reveals both stable ($n < 1$) and unstable (small n_B/N_B when $n > 1$) steady states [Fig. 3(c)].

What happens when the system becomes unstable? As discussed earlier, in fast growth conditions, $\alpha < 1$ in the steady-state initiation mass expression (Eq. 1). Indeed, using numerical simulations, we found that the initiation mass oscillates between two values [Fig. 4(c)]. This indicates that the cell cycle can oscillate between multifork and non-multifork replication. Mathematically, this oscillatory behavior means that the fixed points of $\mathcal{F}^{o2} = \mathcal{F} \circ \mathcal{F}$ are stable, although the fixed point of $\mathcal{F}$ is unstable. By fixing one of the fixed points of $\mathcal{F}^{o2}$ as $\rho_1 = 1$, we can compute the other fixed point with $\rho_1 < 1$ (see Appendix C). In extreme cases, ρ_1 can be as small as 0.1. That is, the second round of replication starts only after 10% of the chromosome has been replicated by the replication forks from the previous initiation. When the replication forks from two consecutive rounds of initiation are too close to each other, they cannot be separated into two division cycles. This should result in two initiation events in one division cycle, and no initiation in the next division cycle.

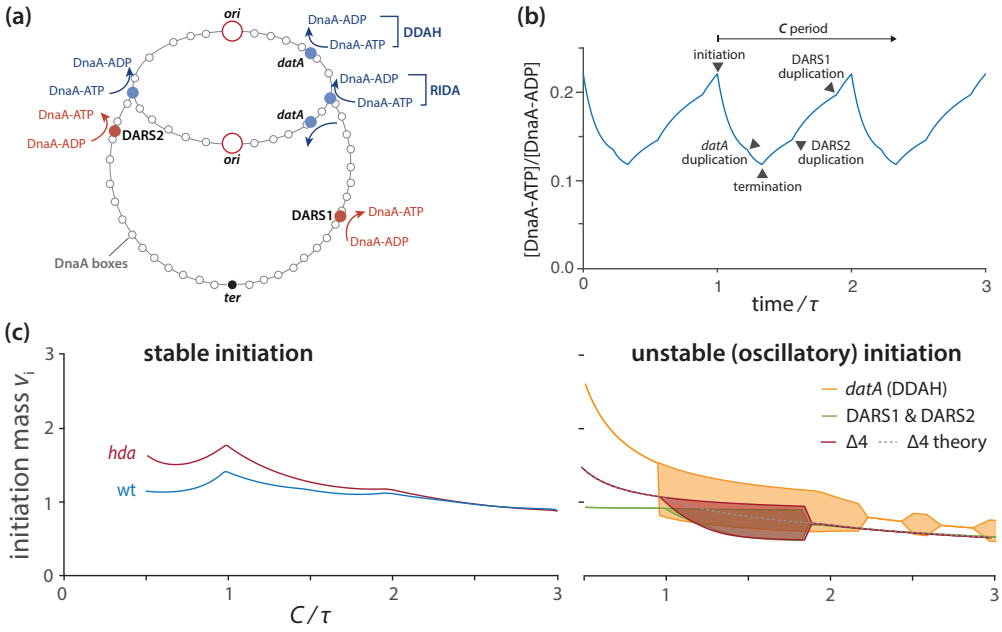

FIG. 5. Initiator-titration model v2 predictions. (a) External DnaA-ATP ↔ DnaA-ADP conversion elements in *E. coli*. (b) [DnaA-ATP]/[DnaA-ADP] changes during the cell cycle predicted by computer simulations. (c) Predicted initiation mass in different growth conditions (C/τ with fixed C). Replication-dependent DnaA-ATP → DnaA-ADP alone can restore stability. None of the other external DnaA-ATP ↔ DnaA-ADP conversion elements can restore the initiation stability. Also see Fig. S3 in Appendix.

D. Replication-dependent DnaA-ATP → DnaA-ADP conversion stabilizes the cell cycle.

When the protocell shows instability, why is the *E. coli* replication cycle stable? *E. coli* has two notable additional features compared to the protocell.

1. As explained in the initiator-titration model v2 earlier, the *E. coli* initiator protein, DnaA, has two forms: DnaA-ATP (active) and DnaA-ADP (inactive) [23]. There are several mechanisms that convert between the two forms of DnaA [13, 17, 18, 24–27].

2. Re-initiation is prevented in *E. coli* within a certain period post-initiation (∼ 10 mins; the "eclipse period"), for example, due to sequestration of newly synthesized DNA by SeqA [13, 28].

These effects have been investigated recently using simulations and modeling [11] and experimentally at the single-cell level [16, 29]. We thus incorporated each of these features into our initiator-titration model v2 based on the protocell model to identify the requirements whereby the instability disappears.

1. *Analytical expression of the initiation mass in the initiator-titration model v2 with a constant DnaA-ATP to DnaA-ADP ratio.*

First, we incorporate the two forms of DnaA into the protocell model to construct the initiator-titration model v2 illustrated in Fig. 2(c). As noted earlier, both DnaA-ATP and DnaA-ADP can bind to the chromosomal DnaA boxes because of their strong binding affinity ($K_D \sim 1$ nM [14, 30, 31]). By contrast, only DnaA-ATP can bind to the weak DnaA boxes at *ori* ($K_D \sim 10^2$ nM [14, 30, 32]). With these assumptions, we can derive an expression for steady-state initiation mass (see Appendix D for details):

$$v_i = \frac{\alpha N_B + (1 + \frac{[\text{DnaA-ADP}]}{[\text{DnaA-ATP}]})n_B}{[\text{DnaA}] - (1 + \frac{[\text{DnaA-ADP}]}{[\text{DnaA-ATP}]})K_{\text{eff}} n_B}, \quad (9)$$

where K_{eff} is the effective dissociation constant of DnaA at *ori*, and α is the same as before in [Eq. 2]. Under physiological conditions, $K_{\text{eff}} n_B \ll [\text{DnaA}]$. Therefore, when [DnaA-ATP] ≫ [DnaA-ADP], the initiation-titration model v2 approaches the protocell model [e.g., Eq. 1]. On the other hand, if [DnaA-ATP] ≪ [DnaA-ADP], there are too few DnaA-ATP compared to the binding sites, and initiation will be critically delayed.

2. *The initiator-titration model 2 also shows instability.*

We investigated the stability of the initiation mass using simulations [Fig. 5(c)]. We found the unstable regime persists when $C/\tau > 1$, slightly larger than the protocell's unstable regime. Importantly, changing the [DnaA-ATP]/[DnaA-ADP] ratio did not significantly impact the stability [Fig. S2(b)].

3. *Replication-dependent DnaA-ATP → DnaA-ADP conversion restores stability.*

Next, we implemented DnaA-ATP → DnaA-ADP and DnaA-ADP → DnaA-ATP conversions in the initiator-titration model v2. In *E. coli*, multiple molecular mechanisms are involved in such conversions [Fig. 5(a)]. Compared to the constant [DnaA-ATP]/[DnaA-ADP] in the

initiator-titration model v2, the replication-dependent DnaA-ATP ↔ DnaA-ADP conversion induces temporal modulations in [DnaA-ATP]/[DnaA-ADP] during cell elongation that peaks at initiation [Fig. 5(b)] [33].

Fig. 5(c) shows the effect of each known conversion element on the stability in initiation. Among these, the DnaA-ATP → DnaA-ADP by RIDA at the replication forks strikingly eliminated the instability regime, while all other conversion elements only had mild effects on the stability [see Fig. S3 for more evidence]. This is likely due to the immediate reduction of DnaA-ATP abundance in the cell by RIDA at the newly-formed replication forks, which should suppress premature re-initiation.

Although DnaA-ATP → DnaA-ADP by RIDA is the key mechanism to stabilize initiation, it significantly reduces the average DnaA-ATP level and delays initiation. Our simulations show that the delayed initiation can be alleviated by the other DnaA-ATP ↔ DnaA-ADP conversion elements without causing instability [Fig. 5(c)]. Interestingly, the initiation mass becomes nearly invariant across a wide range of growth conditions in the presence of all four external conversion elements [Fig. 5(c)].

Based on these results, we conclude that the [DnaA-ATP]/[DnaA-ADP] regulatory mechanisms can significantly enhance the initiation stability and keep the initiation mass nearly constant against physiological perturbations.

4. *The eclipse period or origin sequestration does not improve stability.*

We added the eclipse period to our protocell simulations. During the predefined eclipse period, we did not allow the binding of the initiator to *ori*. Surprisingly, the eclipse period did not improve stability significantly as long as the doubling time is shorter than the C period. However, the amplitude of the initiation mass oscillation decreased slightly [Fig. S4]. Therefore, we predict the effect of SeqA on steady-state stabilization to be modest. While the details of these and other molecular effects on initiation are beyond the scope of this work, we suggest recent work by Berger and ten Wolde for extensive numerical simulations [11] and by Elf and colleagues for single-cell level experimental investigation [29].

E. Stochasticity Part I: asynchrony and intrinsic noise

Initiation stability raises a related issue of stochasticity in initiation. Previously, we implemented the notion of intrinsic vs. extrinsic noise to distinguish asynchrony (intrinsic) vs. cell-to-cell variability (extrinsic) by decomposing the distribution of initiation of multiple *ori*'s along orthogonal axes, as illustrated in Fig. 6(a) [16, 34]. In this section, we discuss their origin and statistical properties within our initiator-titration model v2 framework.

1. *Asynchrony and intrinsic noise.*

During multifork replication, the chromosome contains multiple replication origins. These origins on the same chromosome can initiate asynchronously, and we previously defined them as intrinsic noise [16, 34].

For simplicity, consider two overlapping replication cycles. Suppose each of the two *ori*'s initiates at an initiation mass $v_{\rm i}^{(1)}$ and $v_{\rm i}^{(2)}$, respectively. The intrinsic noise of the initiation mass can be measured by the coefficient of variation as

$$CV_{\rm int}^2 = \frac{\left\langle (v_{\rm i}^{(1)} - v_{\rm i}^{(2)})^2 \right\rangle}{2\left\langle v_{\rm i}^{(1)} \right\rangle \left\langle v_{\rm i}^{(2)} \right\rangle}. \tag{10}$$

In our initiator-titration model framework, each initiation mass is determined by the first passage time (FPT) [35]. That is, the initiator proteins bind the binding sites at *ori*, increasing its occupancy $O(t)$, and initiate replication as soon as *ori* is fully saturated [$O(t) = n_{\rm B}$]. In the zeroth-order approximation, we can treat the initiator accumulation kinetics $O(t)$ at the two *ori*'s as two independent trajectories following Poisson processes. Hence, we have

$$CV_{\rm int} \approx CV_{\rm FPT} = \frac{\sigma_{\rm FPT}}{\langle t_{\rm FPT} \rangle}, \tag{11}$$

where $\langle t_{\rm FPT} \rangle$ is the mean FPT at one *ori* and $\sigma_{\rm FPT}$ is the standard deviation [see Appendix F].

Regardless of model details, the simplest accumulation scenario for $O(t)$ is the Poisson process. We assume a constant accumulation rate β, and the absorbing threshold of the accumulation dynamics $O(t) = N_{\rm th}$. This results in a Gamma distribution of the FPT:

$$P(t_{\rm FPT}; N_{\rm th}, \beta) = \frac{\beta^{N_{\rm th}} t_{\rm FPT}^{N_{\rm th}-1} e^{-\beta t_{\rm FPT}}}{(N_{\rm th}-1)!}, \tag{12}$$

which gives a mean value as $\langle t_{\rm FPT} \rangle = N/\beta$, and a standard deviation as $\sigma_{\rm FPT} = \sqrt{N_{\rm th}}/\beta$. Thus, the $CV_{\rm FPT}$ is independent of β [36],

$$CV_{\rm FPT} = \frac{1}{\sqrt{N_{\rm th}}}. \tag{13}$$

Therefore, in the one-step Poisson process, the only way to suppress the noise is to increase the threshold $N_{\rm th}$. In *E. coli*, the number of binding sites at *ori* is roughly $N_{\rm th} = n_{\rm B} \approx 10$, thus $CV_{\rm FPT} \approx 30\%$ [Fig. 6(a)]. If the cell localizes all $N_{\rm B} \approx 300$ DnaA boxes at *ori* to increase the threshold, the noise would decrease to $CV_{\rm FPT} = 1/\sqrt{300} \approx 6\%$ [Fig. 6(b)].

As we explain below, *E. coli* suppresses the noise using an ingenious two-step Poisson process.

2. *E. coli and the initiator-titration model v2.*

Due to the significant differences in the binding affinity between the chromosomal binding sites ($K_{\rm D} \approx 1$nM)

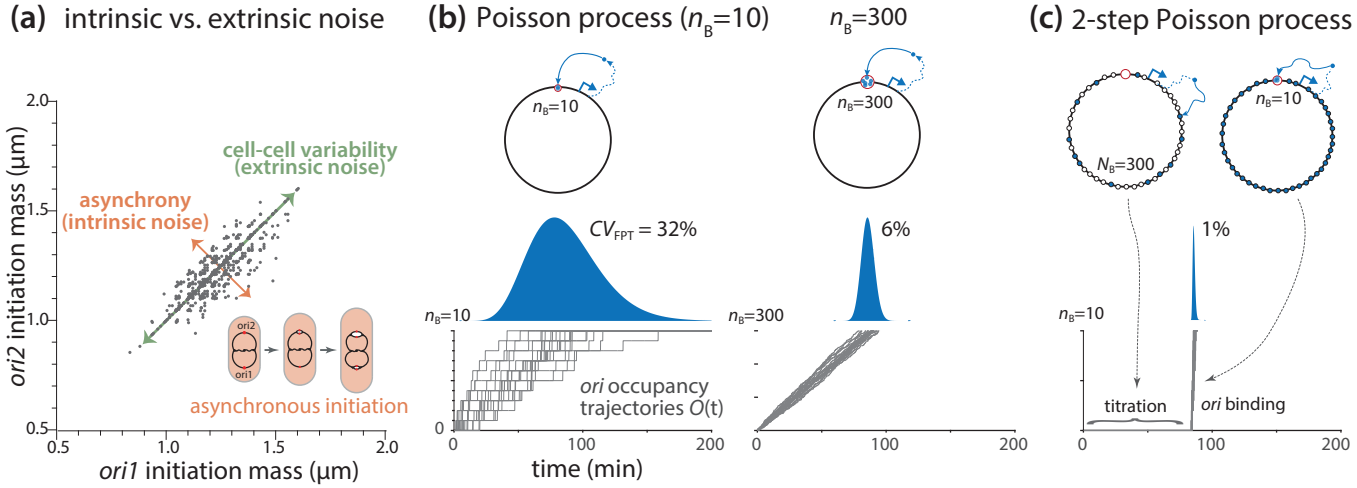

FIG. 6. Initiation noise and the reduction in intrinsic noise by $1/N$ scaling in the two-step Poisson process by titration. (a) Intrinsic noise (asynchrony) vs. extrinsic noise (cell-cell variability) in initiation control. (b) Initiation by the first-passage time of initiator accumulation to a threshold number in bacteria. (left) $n_B = 10$ vs. (right) $n_B = 300$. (c) Dramatic intrinsic noise reduction in the two-step Poisson process.

and at *ori* ($K_D \approx 100$nM), *E. coli* titrates DnaA sequentially in two steps: (1) saturation of the N_B chromosomal DnaA boxes by DnaA-ATP and DnaA-ADP, followed by (2) accumulation of DnaA-ATP at *ori* with $n_B \ll N_B$ binding sites. In other words, titration effectively turns the initiation process into two-step Poisson process [Fig. 6(c)]. In the first step, the DnaA-ATP accumulation at *ori* is nearly zero due to the titration of DnaA by the chromosomal DnaA boxes. This first step dominates the mean FPT, $\langle t_{FPT}\rangle = N_B/\beta$, and stochasticity becomes only significant after the chromosomal DnaA boxes are nearly saturated. In the second step, DnaA-ATP starts saturating the n_B binding sites at *ori* following the Poisson process, which dominates the standard deviation of the initiation time with $\sigma_{FPT} = \sqrt{n_B}/\beta$ [See Appendix F].

These two processes together result in the CV of the total FPT as

$$CV_{FPT} = \frac{\sqrt{n_B}}{N_B}. \tag{14}$$

With $n_B = 10$ and $N_B = 300$, the noise of the two-step processes decreases dramatically to only 1% [Fig. 6(c)]. This reduction in noise is due to the change in the scaling behavior of CV from the one-step Poisson process' $1/\sqrt{N}$ to the two-step Poisson process $1/N$.

3. *Coupling of the two initiation processes by titration.*

The two-step Poisson processes described above predict $CV_{int} \approx 1\%$. In wildtype *E. coli*, CV_{int} is about 3%-4% [16], larger than predicted. We reason that the Poisson processes for the initiator accumulation at the two *ori*'s are negatively correlated. For example, consider the duplication of DnaA boxes after the first initiation. The newly produced DnaA boxes will titrate the DnaA, further delaying the initiation of the second *ori*. This anti-correlation between two asynchronous initiations should increase the intrinsic noise CV_{int}.

In summary, the chromosomal titration boxes effectively synchronize the initiation of multiple *ori*'s [37]. This is consistent with long-standing experimental observations of synchronous initiation of minichromosomes [38], and more recent observations of ectopic chromosomal origins [39]. This improvement of precision by two sequential binding processes is reminiscent of the ratchet-like kinetic proofreading model, and our results are generalizable.

F. Stochasticity Part II: cell-to-cell variability and extrinsic noise.

A population of cells in steady-state growth also exhibits cell-to-cell variability in initiation mass, governed by the extrinsic noise defined by [16, 34]

$$CV^2_{ext} = \frac{\left\langle v_i^{(1)} v_i^{(2)} \right\rangle - \left\langle v_i^{(1)} \right\rangle \left\langle v_i^{(2)} \right\rangle}{\left\langle v_i^{(1)} \right\rangle \left\langle v_i^{(2)} \right\rangle}. \tag{15}$$

Note that the cell-to-cell variability can be caused by both intrinsic noise and extrinsic noise, but in most cases the extrinsic noise prevails. Here, we suggest that the extrinsic noise comes from two parts: the cell-to-cell variability of the parameters in the steady-state initiation mass formula [Eq. 1 or 9], and the bimodal initiation mass caused by the instability of the steady-state. In reality, parameters in our initiator-titration model v2 must have a distribution due to intrinsic stochasticity,

such as the concentration $c_{\rm I}$ [40–42], doubling time τ [9, 43], and the replication period C [6, 44]. A small shift in these parameters can shift the steady-state initiation mass to a new value. Suppose the parameter set is $\{p_{\rm m}\}$, $m = 1, 2, 3, ...$, and assume these parameters independently follow log-normal distributions. The extrinsic noise can then be calculated as

$$CV^2_{\rm ext} = \sum_{\rm m} \left(\frac{\partial \ln v_{\rm i}}{\partial \ln p_{\rm m}}\right)^2 \left(\frac{\delta p_{\rm m}}{p_{\rm m}}\right)^2, \qquad (16)$$

where $\left|\frac{\delta p_{\rm m}}{p_{\rm m}}\right|$ is the noise from the parameter $p_{\rm m}$.

The simplest case is the protocell model with $C/\tau < 1$, where the steady state is always stable. The main source of noise is the initiator concentration. Due to the inverse relationship between $v_{\rm i}$ and $c_{\rm I}$ [Eq. 1], we have

$$CV_{\rm ext} = CV_{c_{\rm I}}. \qquad (17)$$

In *E. coli*, we estimate the noise from DnaA concentration to be approximately 10% [16]. Since this noise originates from the stochasticity in gene expression regardless of other noise sources, the 10% noise should be considered a lower bound. Indeed, this value is comparable to the noise of initiation mass in wild-type *E. coli* and *Bacillus subtilis* [6, 45].

For wildtype *E. coli*, we suggest the stochasticity in gene expression protein production is the major source of extrinsic noise or cell-to-cell variability, as has been studied extensively in the past [40]. For mutant *E. coli* lacking some or all of the external DnaA-ATP ↔ DnaA-ADP elements, the instability can dominate the cell-to-cell variability [16]. We leave a more detailed analysis to future work.

III. CONCLUSION AND PERSPECTIVE

In this work, we have provided a comprehensive quantitative explanation of how bacteria control the cell cycle under balanced growth, particularly focusing on replication initiation as a tractable problem. Our analysis builds upon the original initiator-titration model proposed by Hansen and colleagues [15], which offered valuable insights into the two-step titration processes that trigger initiation.

Over the past three decades, significant progress has been made in understanding the conserved master replication initiator protein, DnaA. One perplexing aspect has been the coexistence of two forms of DnaA (DnaA-ATP and DnaA-ADP), with only DnaA-ATP being initiation competent. Expanding upon the original model by Hansen and colleagues, we developed the initiator-titration model v2, which incorporates the two-state DnaA model and accounts for DnaA box distribution. We have derived an analytical expression for the initiation mass in terms of three mechanistic parameters for DnaA: its concentration, the average ratio [DnaA-ATP]/[DnaA-ADP], and the number of DnaA titration boxes (Eq. 9). However, through our dynamical stability analysis, we have also revealed a previously unexplored instability in initiation within this model [Fig. 4(c)], thereby elucidating recent observations from numerical simulations by Berger and ten Wolde [11]. We have demonstrated that the replication-dependent DnaA-ATP → DnaA-ADP conversion (by RIDA) alone restores initiation stability [46]. Additionally, when considering all extrinsic DnaA-ATP ↔ DnaA-ADP elements, the initiation mass remains remarkably invariant across a wide range of growth conditions, in agreement with experimental observations [21, 47, 48].

Moreover, we have discovered that the titration process of the chromosomal DnaA boxes suppresses intrinsic noise or asynchrony in initiation by a factor of $CV = 1/N$. This finding represents a significant improvement over the naively expected standard coefficient of variation $CV = 1/\sqrt{N}$ for a Poisson process. It underscores the extraordinary consequences of the two-step initiation processes in the initiator-titration models, highlighting the remarkable precision achieved by bacteria. Ultimately, our work sheds light on how bacteria employ a seemingly simple titration-based strategy to solve a fundamental biological problem, distinguishing themselves from eukaryotes. The implications of this research extend beyond the specific biological problem at hand. It raises intriguing questions about the potential prevalence of titration-based precision control in other biological systems. Exploring and uncovering such examples would be of great interest and importance in our understanding of precision control in general and its applications, including the design of synthetic cells.

ACKNOWLEDGMENTS

We thank Flemming Hansen, Tove Atlung, Tsutomu Katayama, Anders Lobner-Olesen, Godefroid Charbon, Thias Boesen, Johan Elf, Dongyang Li, Fangwei Si, Guillaume Le Treut, Cara Jensen, Mareike Berger, Pieter-Rein ten Wode, Alan Leonard, Julia Grimwade, Conrad Woldringh, Charles Helmstetter, and Willie Donachie for many invaluable discussions and exchange of ideas over the years that inspired and helped shape the ideas presented in this work. This work was supported by NSF MCB-2016090 and NIH MIRA (R35GM139622) to SJ.

[1] L. Wolpert, Positional information and the spatial pattern of cellular differentiation, J. Theor. Biol. **25**, 1 (1969).

[2] T. Evans, E. T. Rosenthal, J. Youngblom, D. Distel, and T. Hunt, Cyclin: a protein specified by maternal mRNA in sea urchin eggs that is destroyed at each cleavage division, Cell **33**, 389 (1983).

[3] S. Jun, F. Si, R. Pugatch, and M. Scott, Fundamental principles in bacterial physiology—history, recent progress, and the future with focus on cell size control: a review, Rep. Prog. Phys. **81**, 056601 (2018).

[4] M. Schaechter, O. Maaløe, and N. O. Kjeldgaard, Dependency on medium and temperature of cell size and chemical composition during balanced growth of salmonella typhimurium, Microbiology **19**, 592 (1958).

[5] N. O. Kjeldgaard, O. Maaloe, and M. Schaechter, The transition between different physiological states during balanced growth of salmonella typhimurium, J. Gen. Microbiol. **19**, 607 (1958).

[6] F. Si, G. Le Treut, J. T. Sauls, S. Vadia, P. A. Levin, and S. Jun, Mechanistic origin of Cell-Size control and homeostasis in bacteria, Curr. Biol. **29**, 1760 (2019).

[7] T. den Blaauwen, L. W. Hamoen, and P. A. Levin, The divisome at 25: the road ahead, Curr. Opin. Microbiol. (2017).

[8] M. Campos, I. V. Surovtsev, S. Kato, A. Paintdakhi, B. Beltran, S. E. Ebmeier, and C. Jacobs-Wagner, A constant size extension drives bacterial cell size homeostasis, Cell **159**, 1433 (2014).

[9] S. Taheri-Araghi, S. Bradde, J. T. Sauls, N. S. Hill, P. A. Levin, J. Paulsson, M. Vergassola, and S. Jun, Cell-Size control and homeostasis in bacteria, Curr. Biol. **25**, 385 (2015).

[10] S. Jun and S. Taheri-Araghi, Cell-size maintenance: universal strategy revealed, Trends Microbiol. **23**, 4 (2015).

[11] M. Berger and P. R. T. Wolde, Robust replication initiation from coupled homeostatic mechanisms, Nat. Commun. **13**, 6556 (2022).

[12] A. C. Leonard, P. Rao, R. P. Kadam, and J. E. Grimwade, Changing perspectives on the role of DnaA-ATP in orisome function and timing regulation, Front. Microbiol. **10**, 2009 (2019).

[13] T. Katayama, K. Kasho, and H. Kawakami, The DnaA cycle in escherichia coli: Activation, function and inactivation of the initiator protein, Front. Microbiol. **8**, 2496 (2017).

[14] F. G. Hansen and T. Atlung, The DnaA tale, Front. Microbiol. **9**, 319 (2018).

[15] F. G. Hansen, B. B. Christensen, and T. Atlung, The initiator titration model: computer simulation of chromosome and minichromosome control, Res. Microbiol. **142**, 161 (1991).

[16] T. Boesen, G. Charbon, H. Fu, C. Jensen, D. Li, S. Jun, and others, Robust control of replication initiation in the absence of DnaA-ATP DnaA-ADP regulatory elements in escherichia coli, bioRxiv (2022).

[17] T. Katayama, T. Kubota, K. Kurokawa, E. Crooke, and K. Sekimizu, The initiator function of DnaA protein is negatively regulated by the sliding clamp of the e. coli chromosomal replicase, Cell **94**, 61 (1998).

[18] J. Kato and T. Katayama, Hda, a novel DnaA-related protein, regulates the replication cycle in escherichia coli, EMBO J. **20**, 4253 (2001).

[19] A. C. Leonard and J. E. Grimwade, The orisome: structure and function, Front. Microbiol. **6**, 545 (2015).

[20] L. Riber, J. Frimodt-Møller, G. Charbon, and A. Løbner-Olesen, Multiple DNA binding proteins contribute to timing of chromosome replication in e. coli, Front Mol Biosci **3**, 29 (2016).

[21] F. Si, D. Li, S. E. Cox, J. T. Sauls, O. Azizi, C. Sou, A. B. Schwartz, M. J. Erickstad, Y. Jun, X. Li, and S. Jun, Invariance of initiation mass and predictability of cell size in escherichia coli, Curr. Biol. **27**, 1278 (2017).

[22] S. Cooper and C. E. Helmstetter, Chromosome replication and the division cycle of escherichia colibr, J. Mol. Biol. (1968).

[23] C. Speck, C. Weigel, and W. Messer, ATP- and ADP-dnaA protein, a molecular switch in gene regulation, EMBO J. **18**, 6169 (1999).

[24] R. Kitagawa, H. Mitsuki, T. Okazaki, and T. Ogawa, A novel DnaA protein-binding site at 94.7 min on the escherichia coli chromosome, Mol. Microbiol. **19**, 1137 (1996).

[25] K. Kasho and T. Katayama, DnaA binding locus *datA* promotes DnaA-ATP hydrolysis to enable cell cycle-coordinated replication initiation, Proceedings of the National Academy of Sciences **110**, 936 (2013).

[26] K. Fujimitsu, T. Senriuchi, and T. Katayama, Specific genomic sequences of e. coli promote replicational initiation by directly reactivating ADP-DnaA, Genes Dev. **23**, 1221 (2009).

[27] K. Kasho, K. Fujimitsu, T. Matoba, T. Oshima, and T. Katayama, Timely binding of IHF and fis to DARS2 regulates ATP-DnaA production and replication initiation, Nucleic Acids Res. **42**, 13134 (2014).

[28] M. Lu, J. L. Campbell, E. Boye, and N. Kleckner, SeqA: a negative modulator of replication initiation in e. coli, Cell **77**, 413 (1994).

[29] A. Knöppel, O. Broström, K. Gras, J. Elf, and D. Fange, Regulatory elements coordinating initiation of chromosome replication to the *Escherichia coli* cell cycle, Proceedings of the National Academy of Sciences **120**, e2213795120 (2023).

[30] S. Schaper and W. Messer, Interaction of the initiator protein DnaA of escherichia coli with its DNA target, J. Biol. Chem. **270**, 17622 (1995).

[31] F. G. Hansen, B. B. Christensen, C. B. Nielsen, and T. Atlung, Insights into the quality of DnaA boxes and their cooperativity, J. Mol. Biol. **355**, 85 (2006).

[32] T. A. Rozgaja, J. E. Grimwade, M. Iqbal, C. Czerwonka, M. Vora, and A. C. Leonard, Two oppositely oriented arrays of low-affinity recognition sites in oric guide progressive binding of DnaA during escherichia coli pre-RC assembly, Mol. Microbiol. **82**, 475 (2011).

[33] W. D. Donachie and G. W. Blakely, Coupling the initiation of chromosome replication to cell size in escherichia coli, Curr. Opin. Microbiol. **6**, 146 (2003).

[34] M. B. Elowitz, A. J. Levine, E. D. Siggia, and P. S. Swain, Stochastic gene expression in a single cell, Science **297**, 1183 (2002).

[35] K. R. Ghusinga, J. J. Dennehy, and A. Singh, First-passage time approach to controlling noise in the tim-

ing of intracellular events, Proceedings of the National Academy of Sciences **114**, 693 (2017).

[36] P. P. Pandey, H. Singh, and S. Jain, Exponential trajectories, cell size fluctuations, and the adder property in bacteria follow from simple chemical dynamics and division control, Phys. Rev. E **101**, 062406 (2020).

[37] M. Wallden, D. Fange, E. G. Lundius, Ö. Baltekin, and J. Elf, The synchronization of replication and division cycles in individual e. coli cells, Cell **166**, 729 (2016).

[38] C. E. Helmstetter and A. C. Leonard, Coordinate initiation of chromosome and minichromosome replication in escherichia coli, J. Bacteriol. **169**, 3489 (1987).

[39] X. Wang, C. Lesterlin, R. Reyes-Lamothe, G. Ball, and D. J. Sherratt, Replication and segregation of an escherichia coli chromosome with two replication origins, Proc. Natl. Acad. Sci. U. S. A. **108**, E243 (2011).

[40] Y. Taniguchi, P. J. Choi, G.-W. Li, H. Chen, M. Babu, J. Hearn, A. Emili, and X. Sunney Xie, Quantifying e. coli proteome and transcriptome with Single-Molecule sensitivity in single cells, Science (2010).

[41] H. Salman, N. Brenner, C.-K. Tung, N. Elyahu, E. Stolovicki, L. Moore, A. Libchaber, and E. Braun, Universal protein fluctuations in populations of microorganisms, Phys. Rev. Lett. **108**, 238105 (2012).

[42] P. Wang, L. Robert, J. Pelletier, W. L. Dang, F. Taddei, A. Wright, and S. Jun, Robust growth of escherichia coli, Curr. Biol. **20**, 1099 (2010).

[43] M. Schaechter, J. P. Williamson, J. R. Hood, Jr, and A. L. Koch, Growth, cell and nuclear divisions in some bacteria, J. Gen. Microbiol. **29**, 421 (1962).

[44] G. Le Treut, F. Si, D. Li, and S. Jun, Quantitative examination of five stochastic Cell-Cycle and Cell-Size control models for escherichia coli and bacillus subtilis, Front. Microbiol. **12**, 721899 (2021).

[45] J. T. Sauls, S. E. Cox, Q. Do, V. Castillo, Z. Ghulam-Jelani, and S. Jun, Control of bacillus subtilis replication initiation during physiological transitions and perturbations, MBio **10** (2019).

[46] L. Riber, J. A. Olsson, R. B. Jensen, O. Skovgaard, S. Dasgupta, M. G. Marinus, and A. Løbner-Olesen, Hda-mediated inactivation of the DnaA protein and dnaa gene autoregulation act in concert to ensure homeostatic maintenance of the escherichia coli chromosome, Genes Dev. **20**, 2121 (2006).

[47] H. Zheng, Y. Bai, M. Jiang, T. A. Tokuyasu, X. Huang, F. Zhong, Y. Wu, X. Fu, N. Kleckner, T. Hwa, and C. Liu, General quantitative relations linking cell growth and the cell cycle in escherichia coli, Nat Microbiol **5**, 995 (2020).

[48] W. D. Donachie, Relationship between cell size and time of initiation of DNA replication, Nature **219**, 1077 (1968).

[49] K. Sekimizu, D. Bramhill, and A. Kornberg, ATP activates dnaa protein in initiating replication of plasmids bearing the origin of the e. coli chromosome, Cell **50**, 259 (1987).